Supporting Information

for

Reaction of a non-heme iron-nitrosyl with dioxygen: Decomposition of the ligand through NOD-like activity

Riya Ghosh, Rakesh Mazumdar, Bapan Samanta, Shankhadeep Saha, and Biplab Mondal

Department of Chemistry, Indian Institute of Technology Guwahati, Assam – 781039, India.
Email: biplab@iitg.ac.in; Phone: (+)91-361-258-2317; Fax: (+)91-361-258-2339

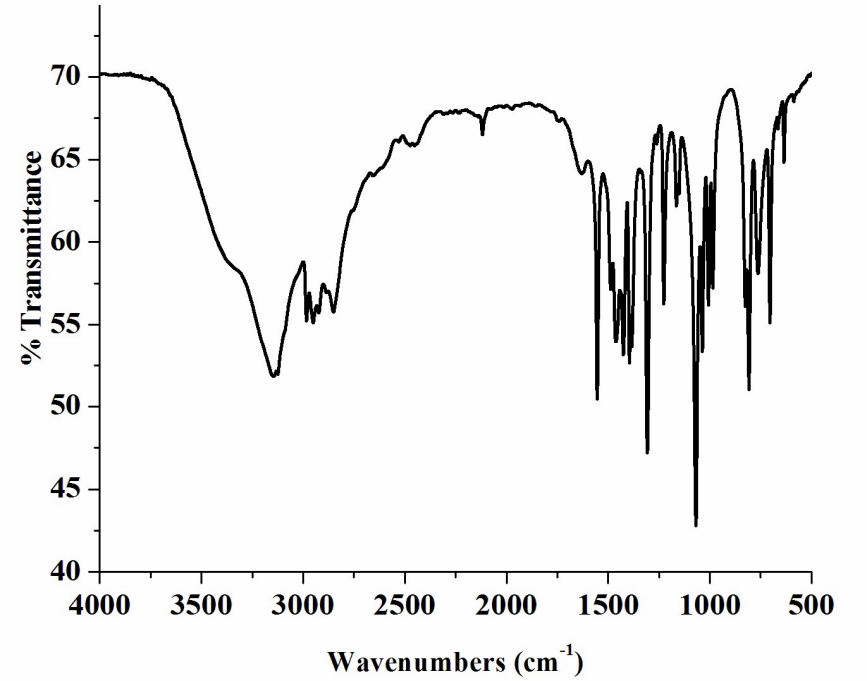

Figure S1: FT-IR spectrum of 1-(hydroxymethyl)-3,5-dimethyl-1-pyrazole in KBr.

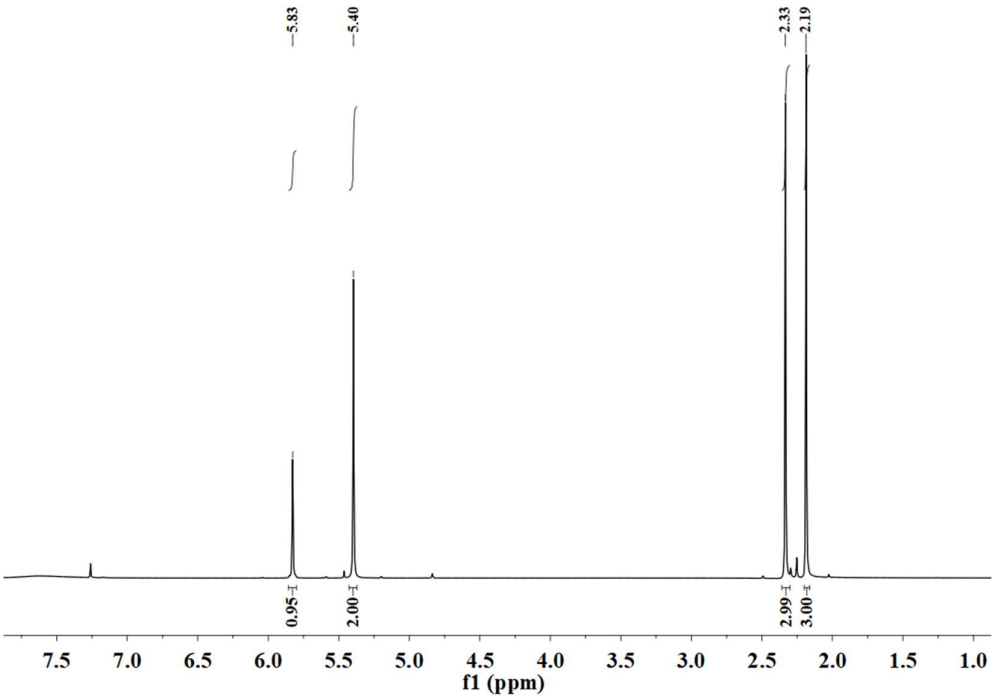

Figure S2: ^{1}H NMR spectrum of 1-(hydroxymethyl)-3,5-dimethyl-1-pyrazole in $CDCl_3$.

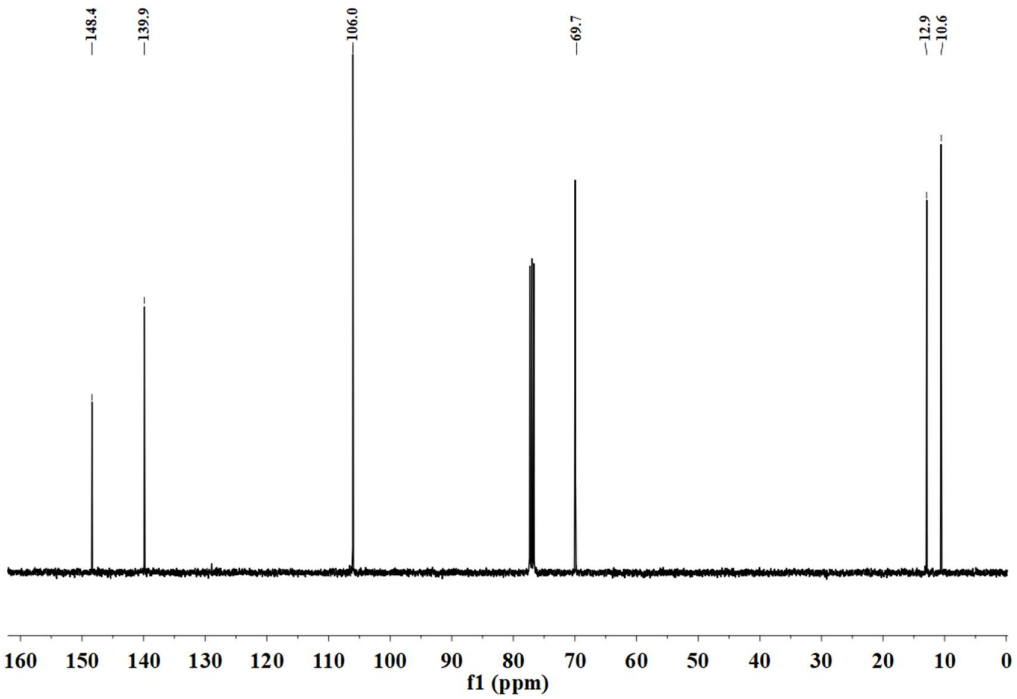

Figure S3: ^{13}C NMR spectrum of 1-(hydroxymethyl)-3,5-dimethyl-1-pyrazole in $CDCl_3$.

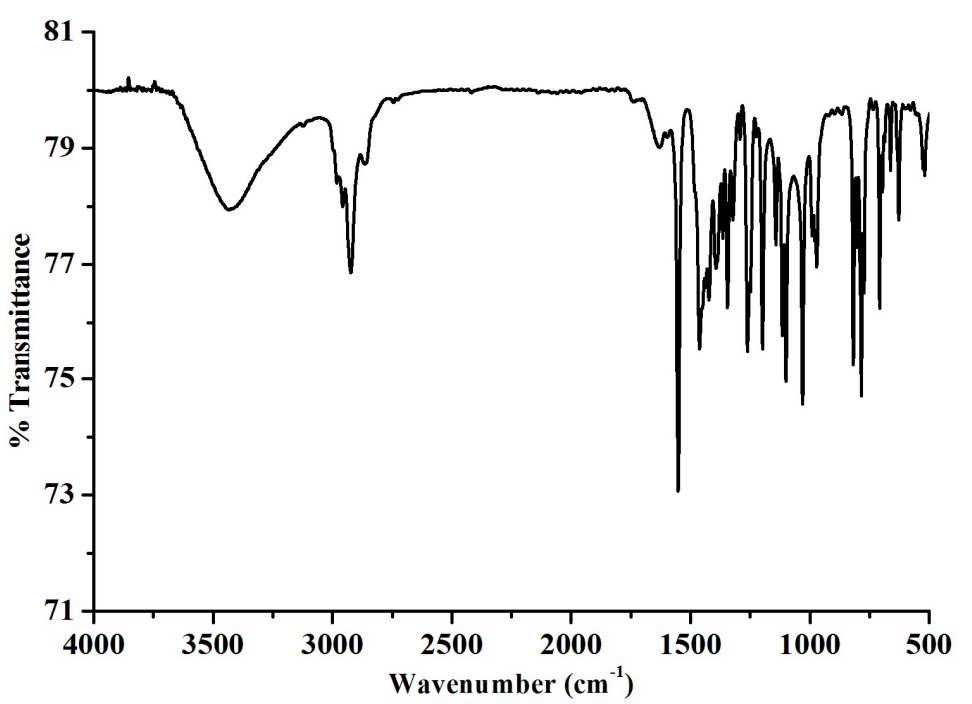

Figure S4: FT-IR spectrum of **TPz** in KBr.

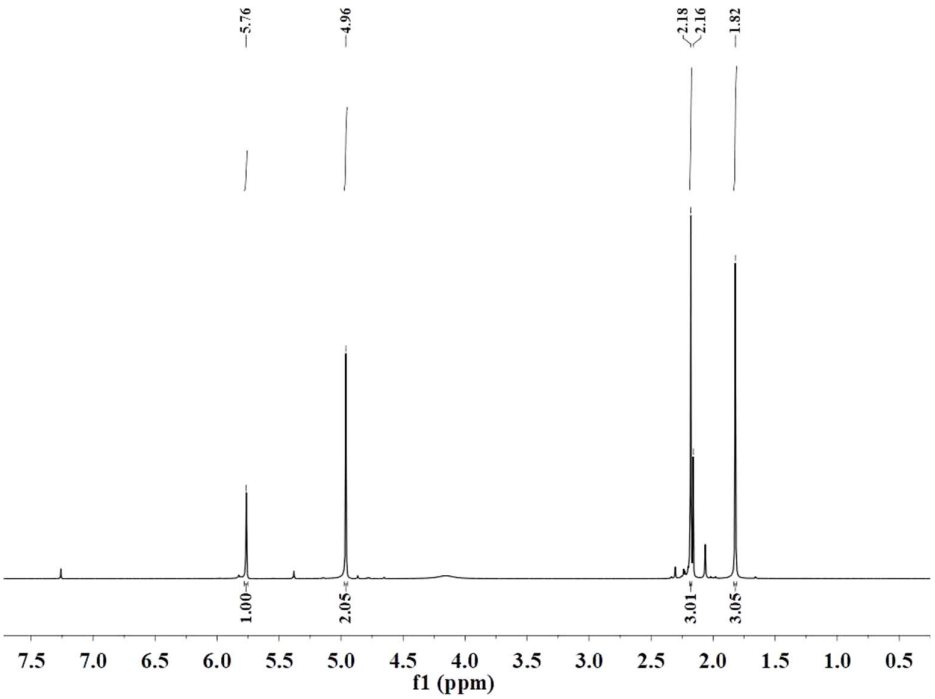

Figure S5: ^{1}H NMR spectrum of **TPz** in $CDCl_3$.

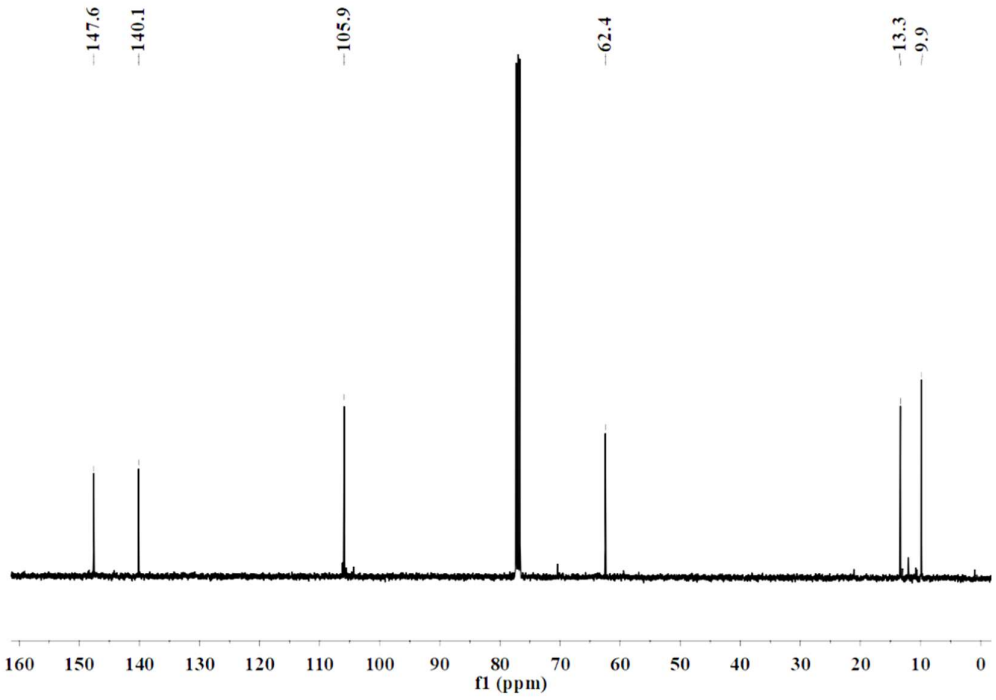

Figure S6: ^{13}C NMR spectrum of **Tpz** in $CDCl_3$.

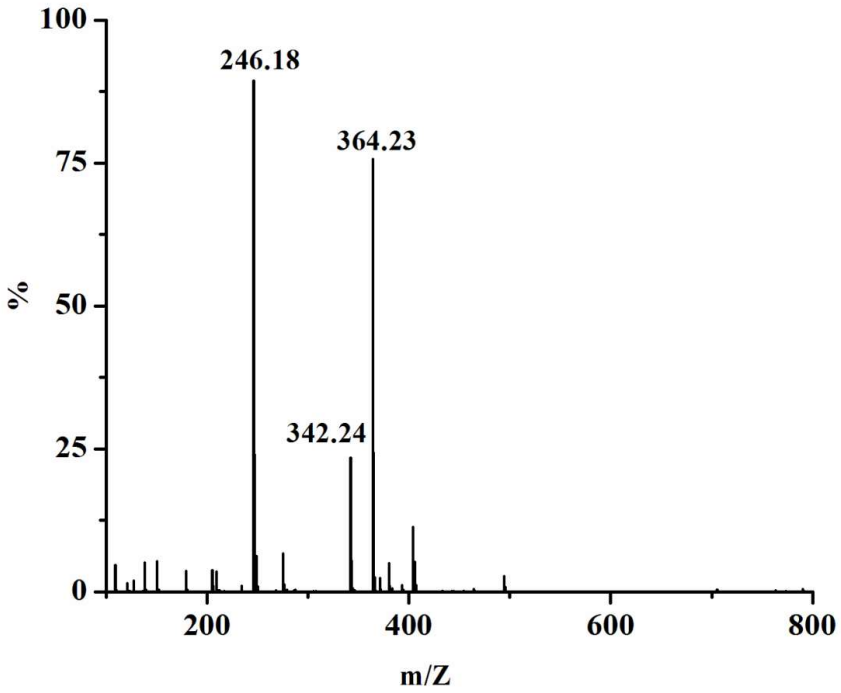

Figure S7: ESI-mass spectrum of ligand **TPz** in acetonitrile.

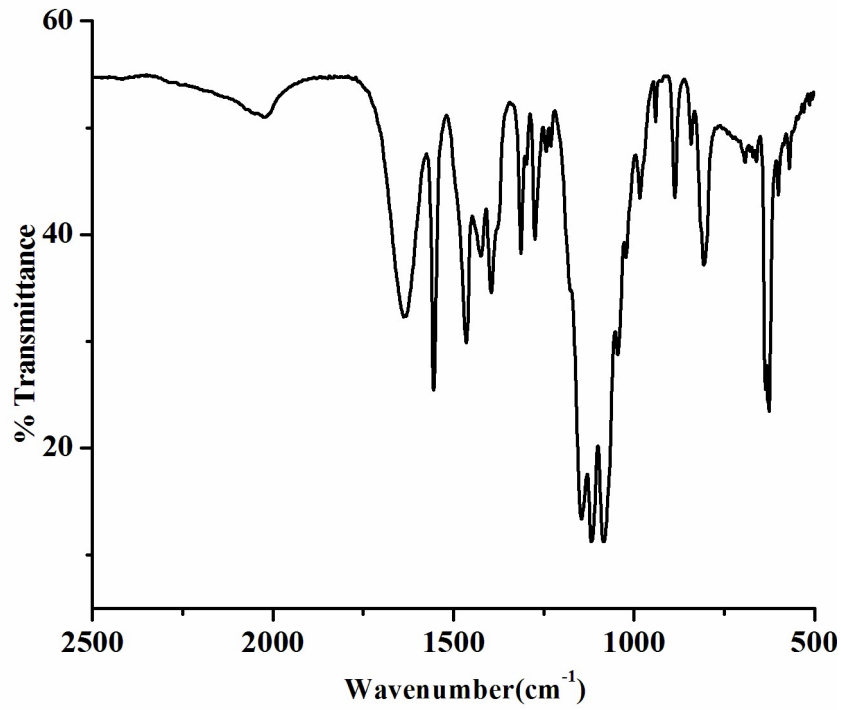

Figure S8: FT-IR spectrum of complex **1** in KBr.

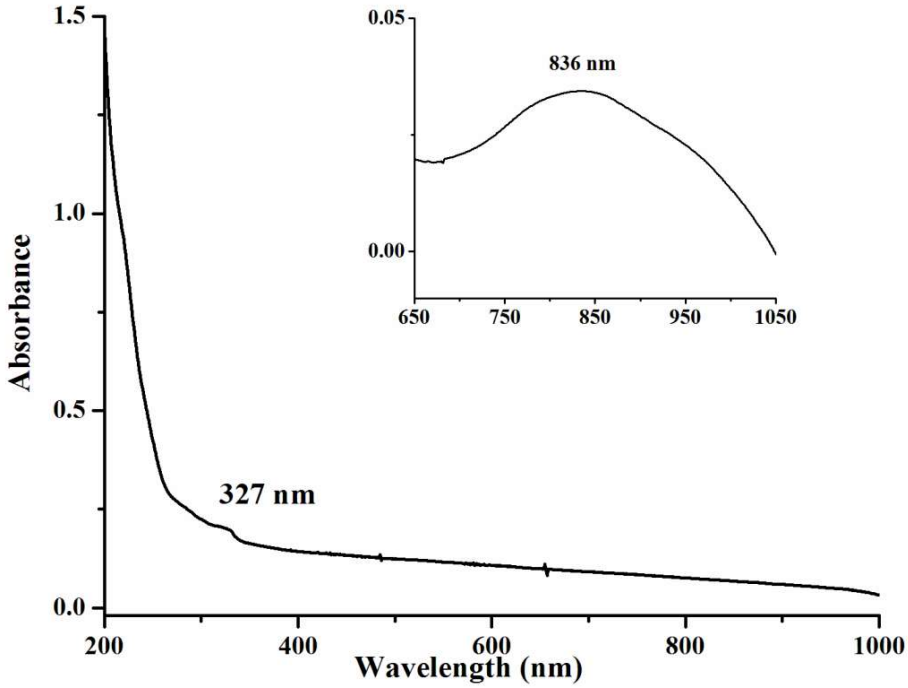

Figure S9: UV-visible spectrum of complex **1** in acetonitrile at RT.

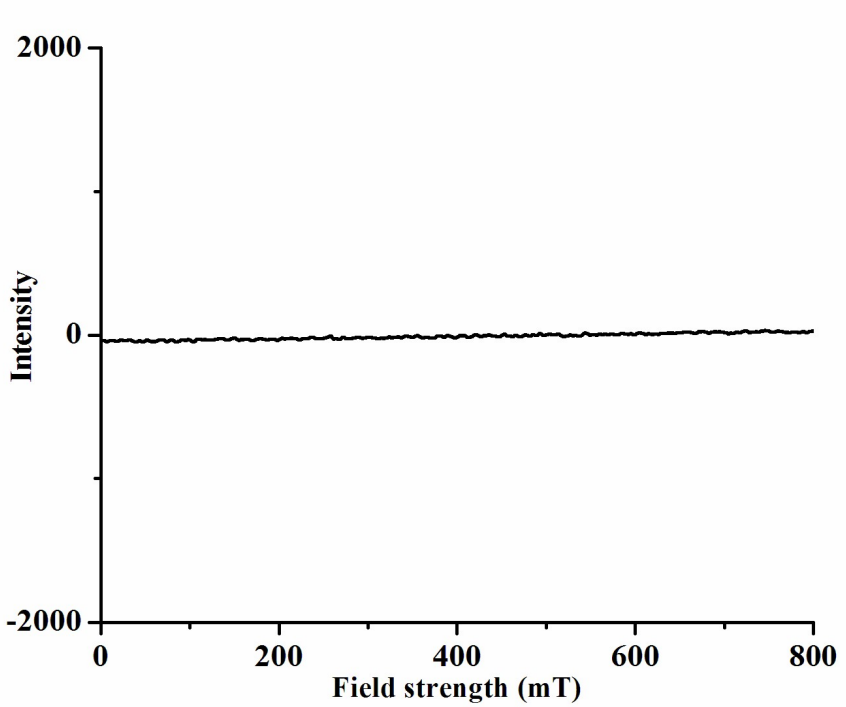

Figure S10: X-band EPR spectrum of complex **1** in acetonitrile at 77 K.

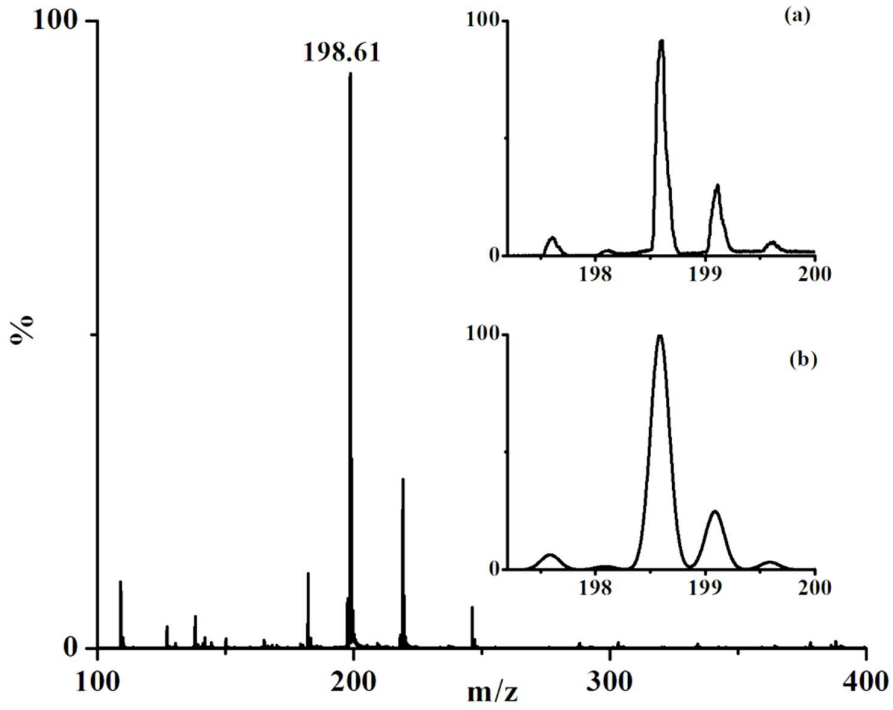

Figure S11: ESI-mass of complex **1** in acetonitrile. [Inset: (a) experimental and (b) simulated isotopic distribution pattern].

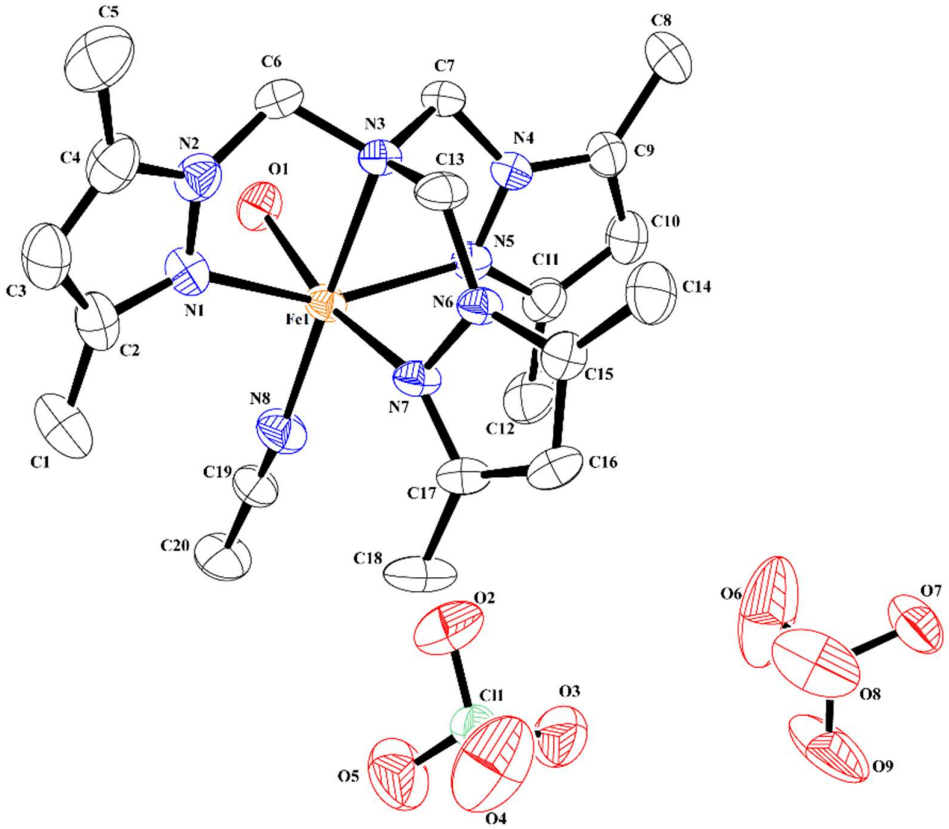

Figure S12. ORTEP diagram of complex 1 (30% thermal ellipsoid plot, H atoms are omitted for clarity).

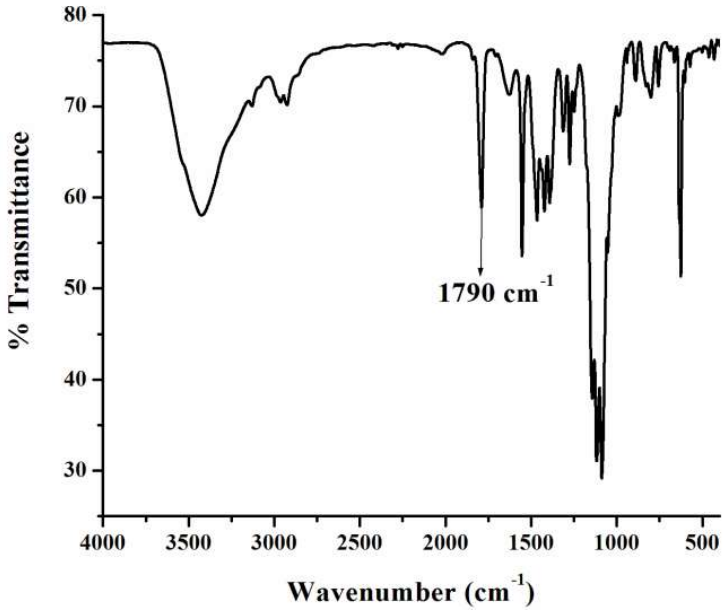

Figure S13: FT-IR spectrum of complex **2** in KBr pellet.

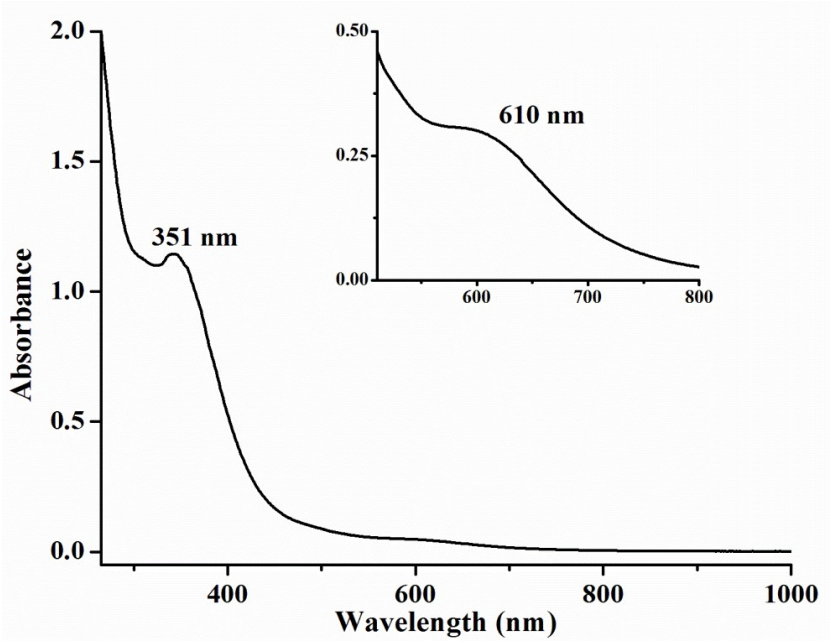

Figure S14: UV-visible spectrum of complex **2** in acetonitrile at RT.

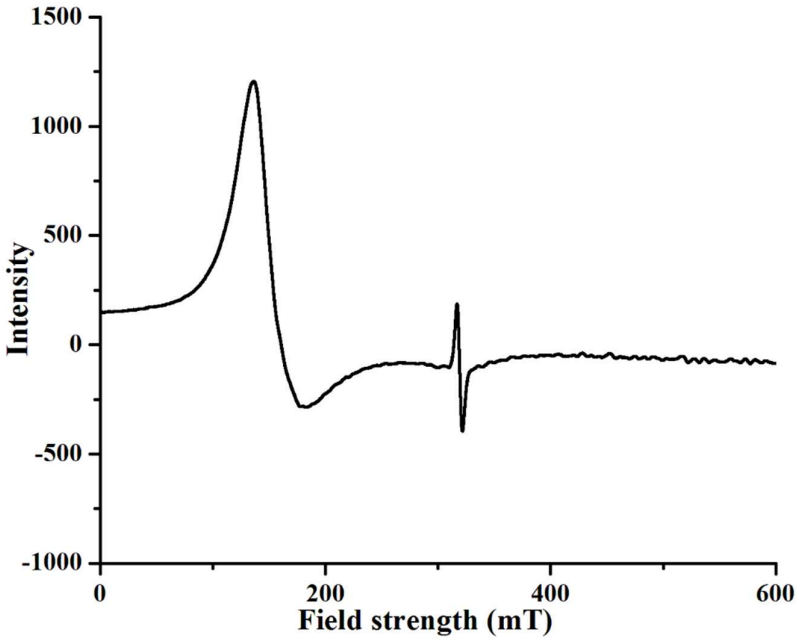

Figure **S15:** X-band EPR spectrum of complex **2** in methanol at 77K.

[Note: a very small amount impurity (< 0.5%) accounting for the isotropic signal near g = 2 in the EPR spectrum]

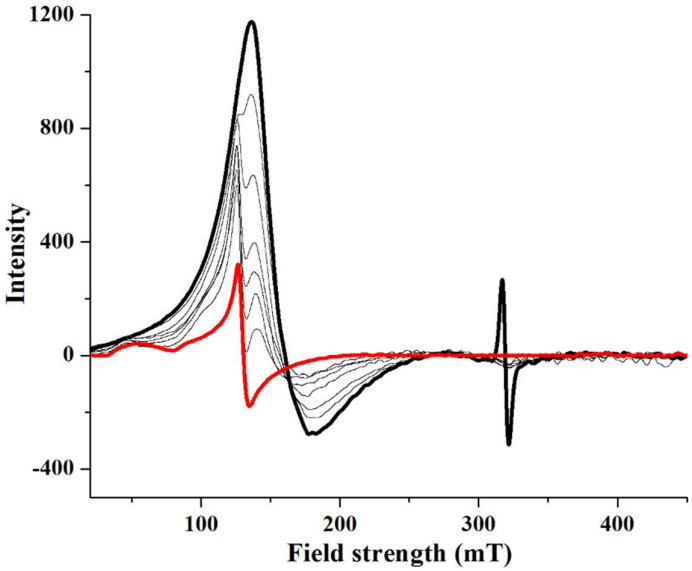

Figure **S16:** X-band EPR Spectra of reaction of complex **2** with O_2 at 77 K in methanol medium. [Complex 2 (black) at g ~ 4.11 and 2.04, after O_2 addition final product (red) at g ~ 5.05].

[Note: a very small amount impurity (< 0.5%) accounting for the isotropic signal near g = 2 in the EPR spectrum]

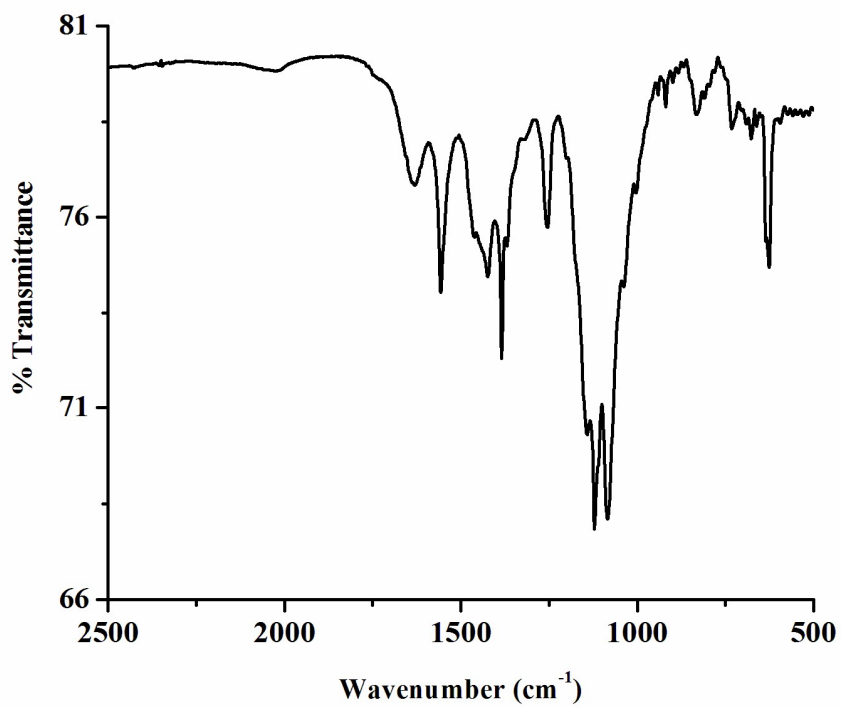

Figure S17: FT-IR spectrum of complex **3** in KBr.

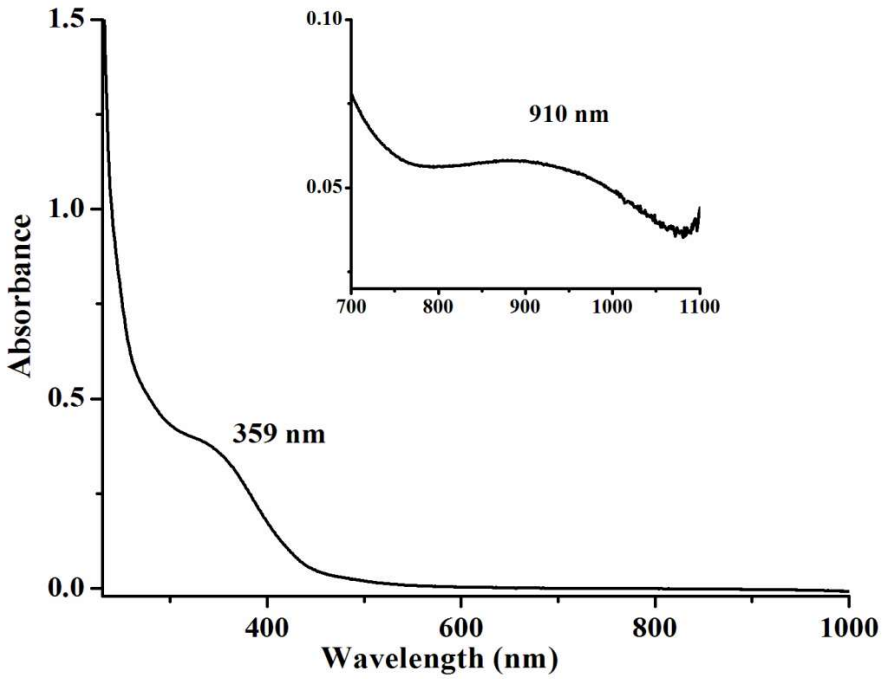

Figure S18: UV-visible spectrum of complex **3** in DMSO at RT.

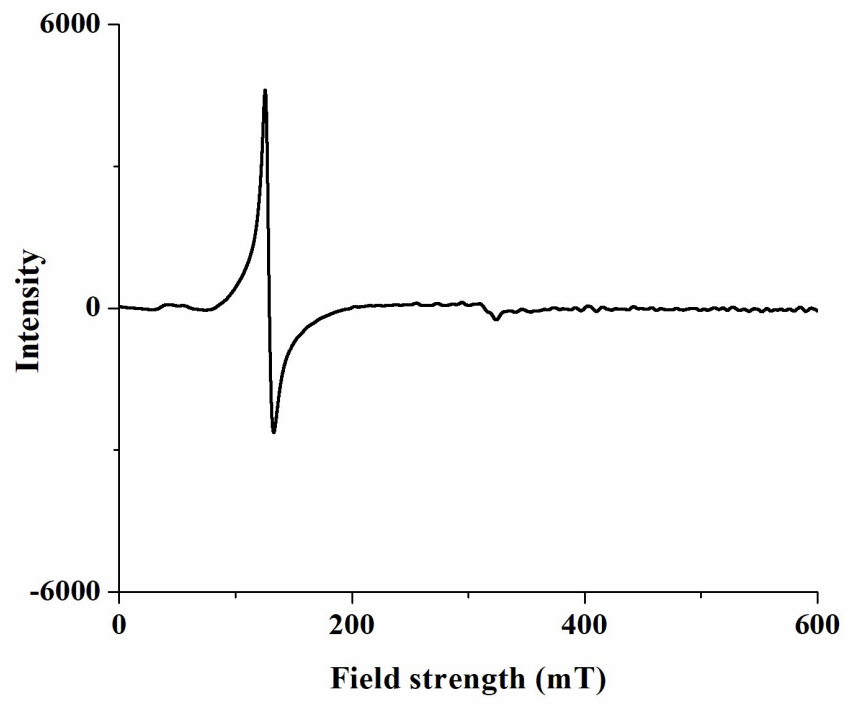

Figure S19: X-band EPR spectrum of complex **3** in DMSO at 77 K (g ~ 5.05).

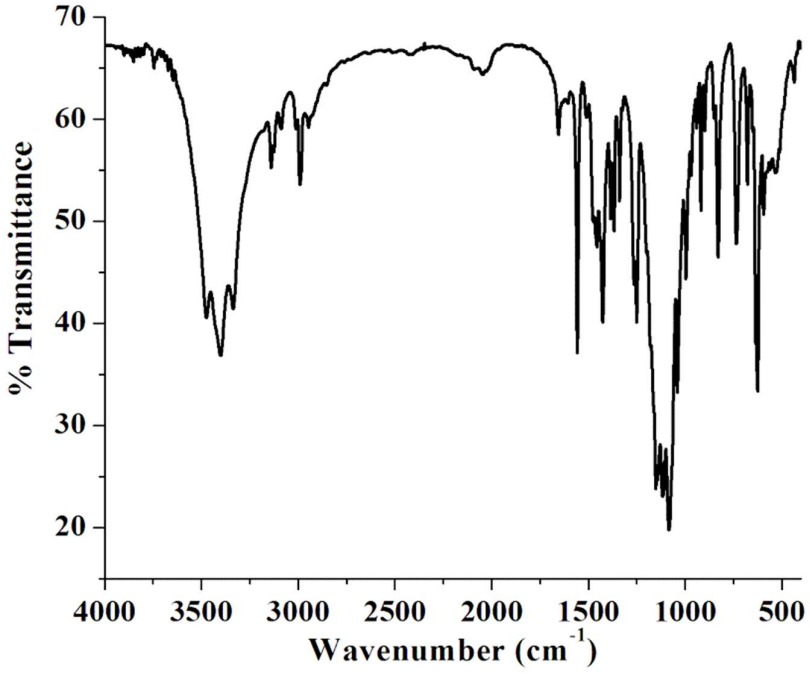

Figure S20: FT-IR spectrum of **L′** in KBr.

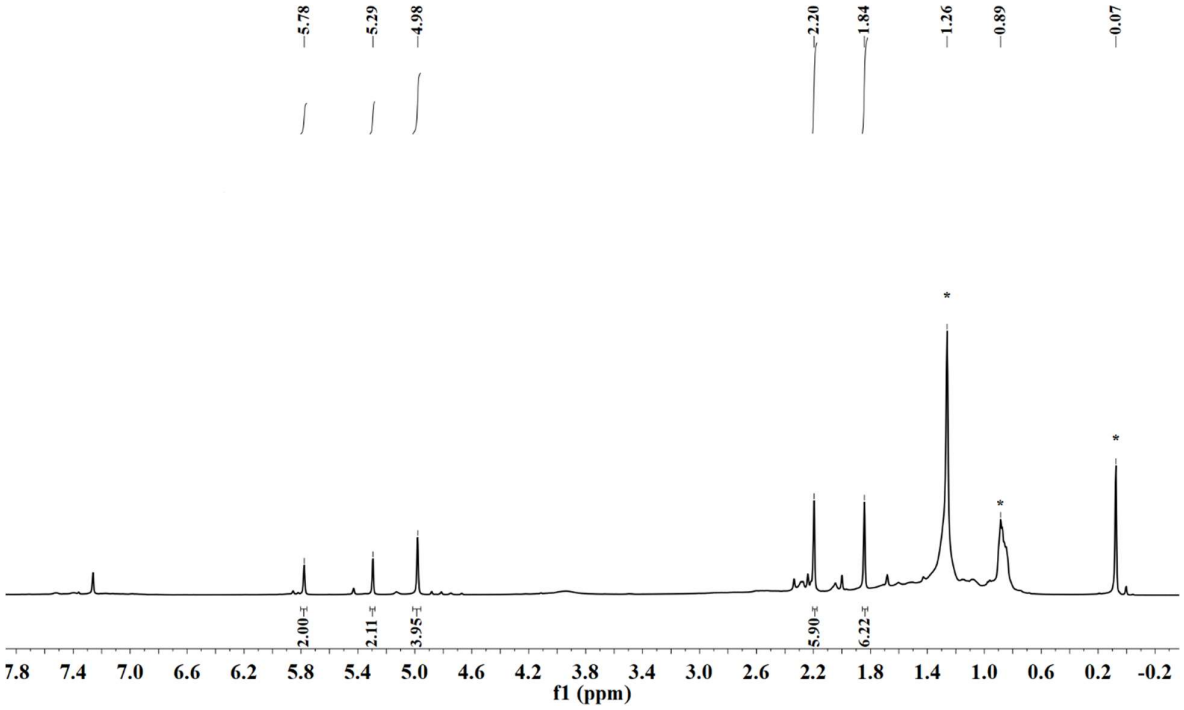

Figure S21: ^{1}H NMR spectrum of modified crystal **L´** in $CDCl_3$. (* for solvent)

.

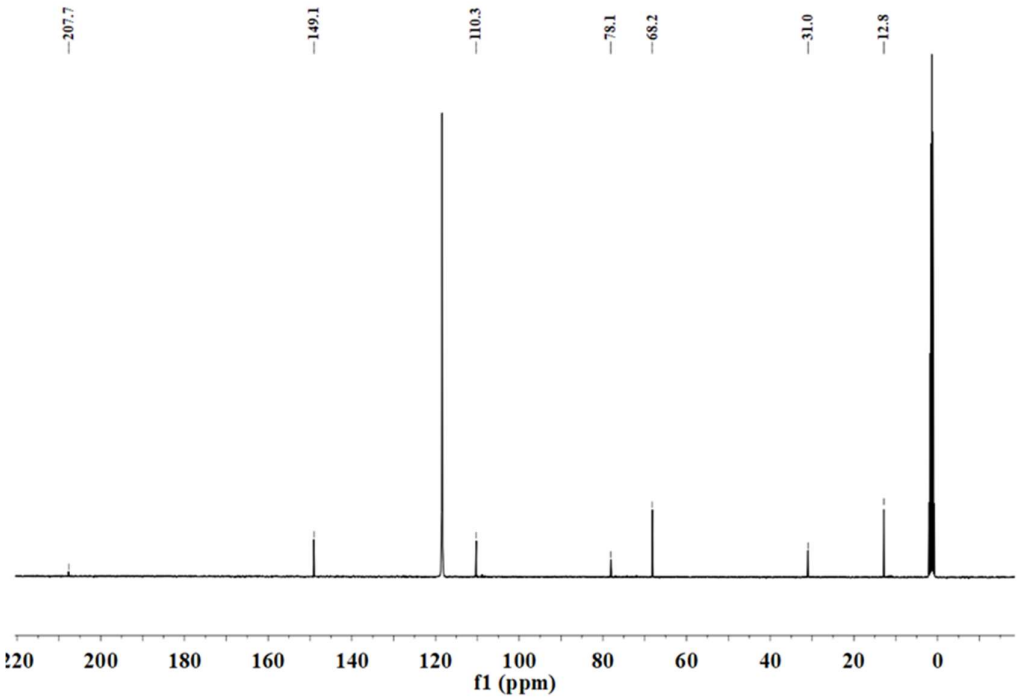

Figure S22: ^{13}C NMR spectrum of **L′** in CD_3CN.

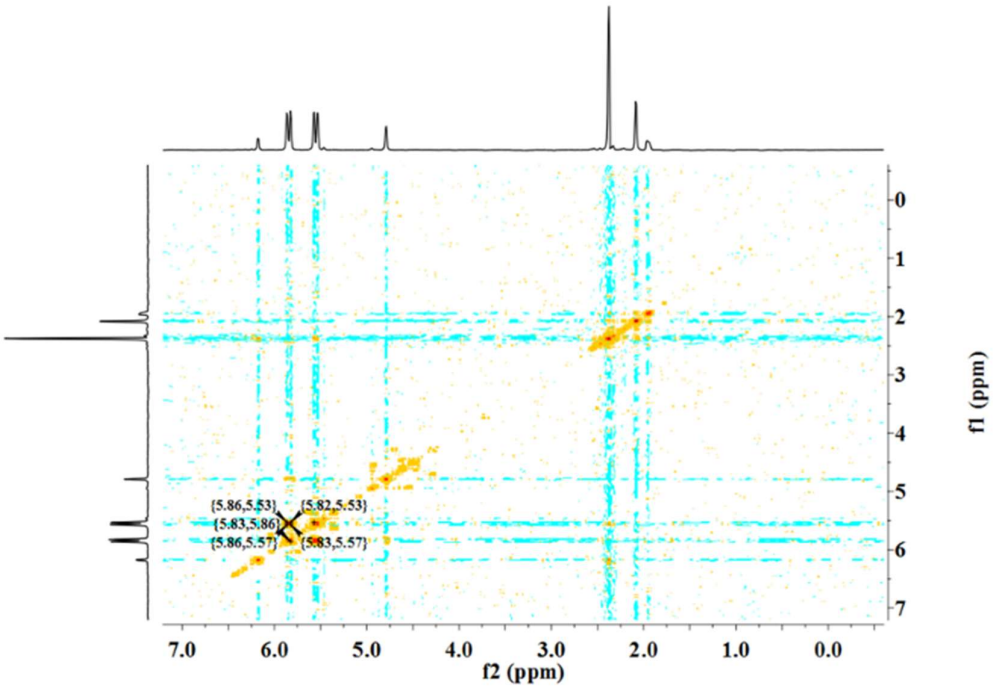

Figure S23: COSY NMR spectrum of **L′** in CD_3CN.

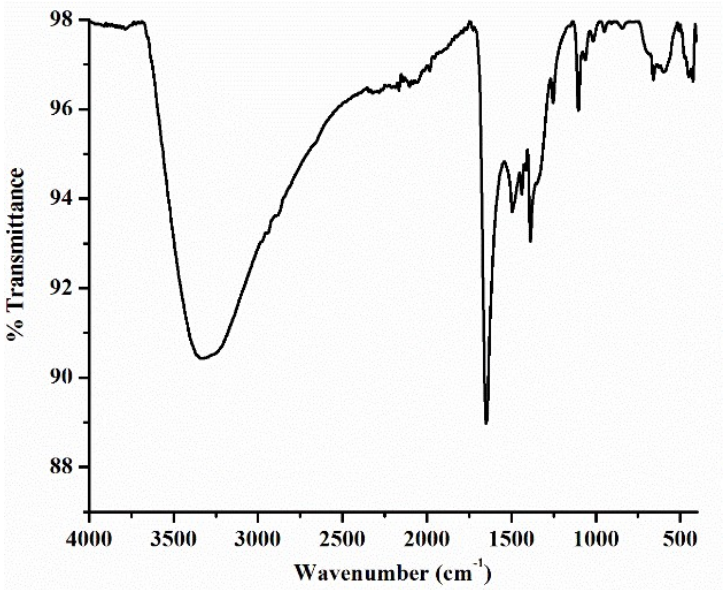

Figure S24: FT-IR spectrum of complex **4** in ATR.

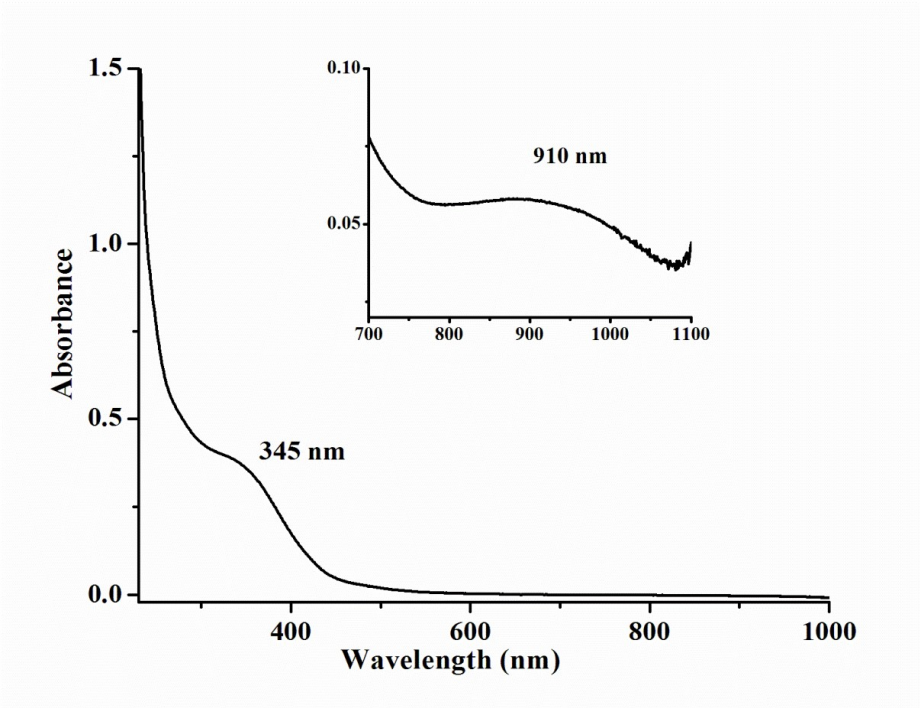

Figure S25: UV-visible spectrum of complex **4** in DMSO at RT.

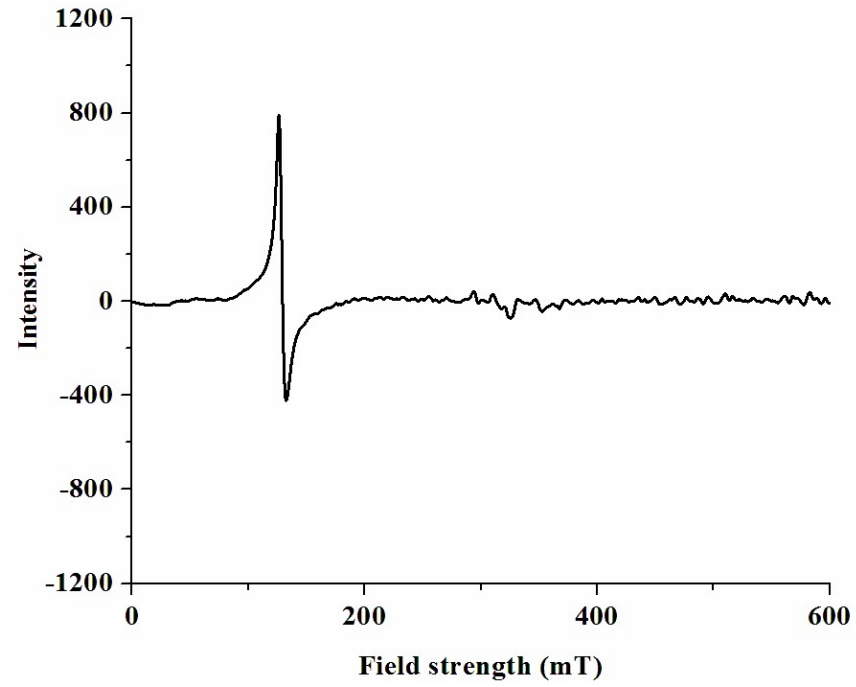

Figure S26: X-band EPR spectrum of complex **4** in DMSO at 77 K (g ~ 5.04).

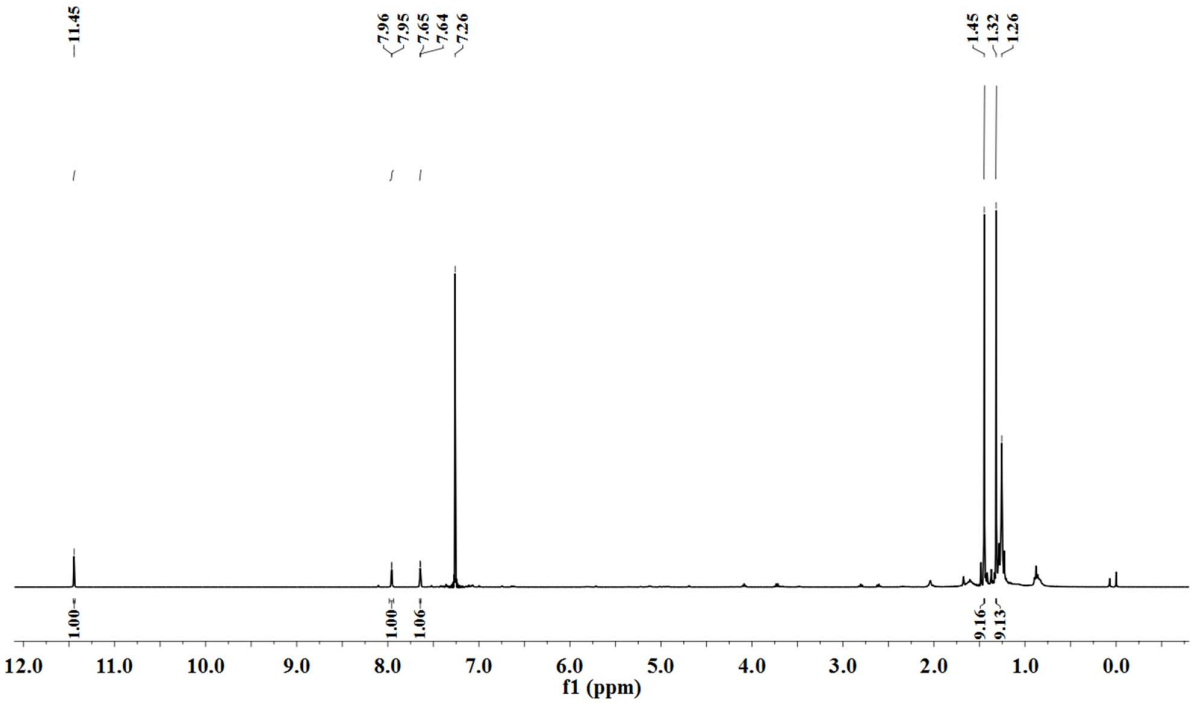

Figure S27: ^{1}H NMR spectrum of 2,4-di-*tert*-butyl-6-nitrophenol in $CDCl_3$.

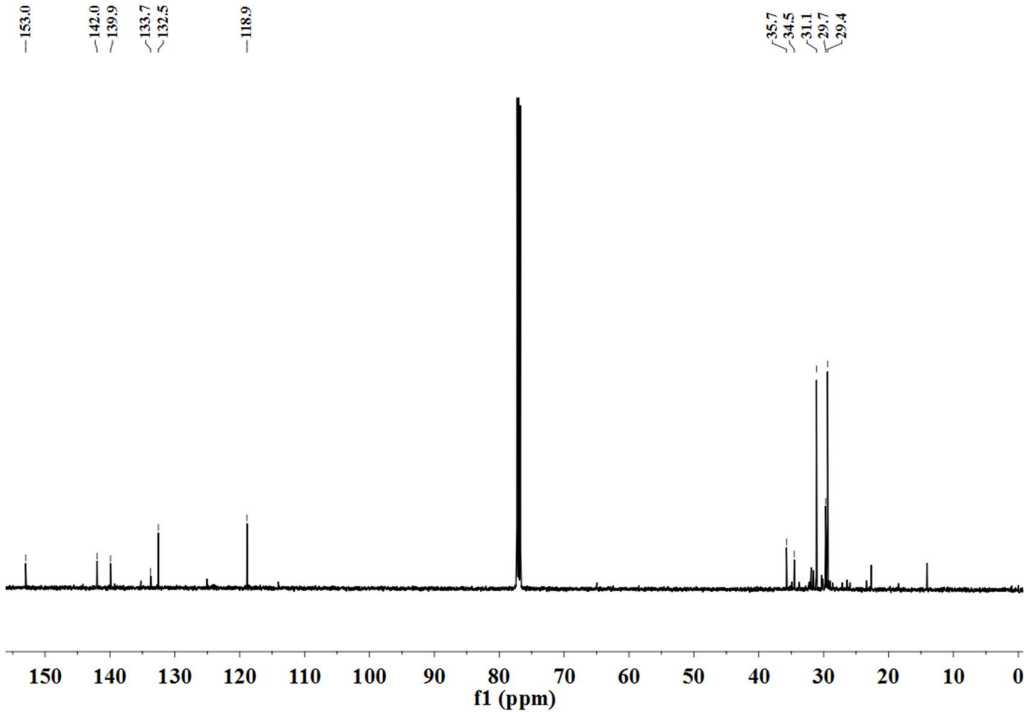

Figure S28: ^{13}C NMR spectrum of 2, 4-di-*tert*-butyl-6-nitrophenol in $CDCl_3$.

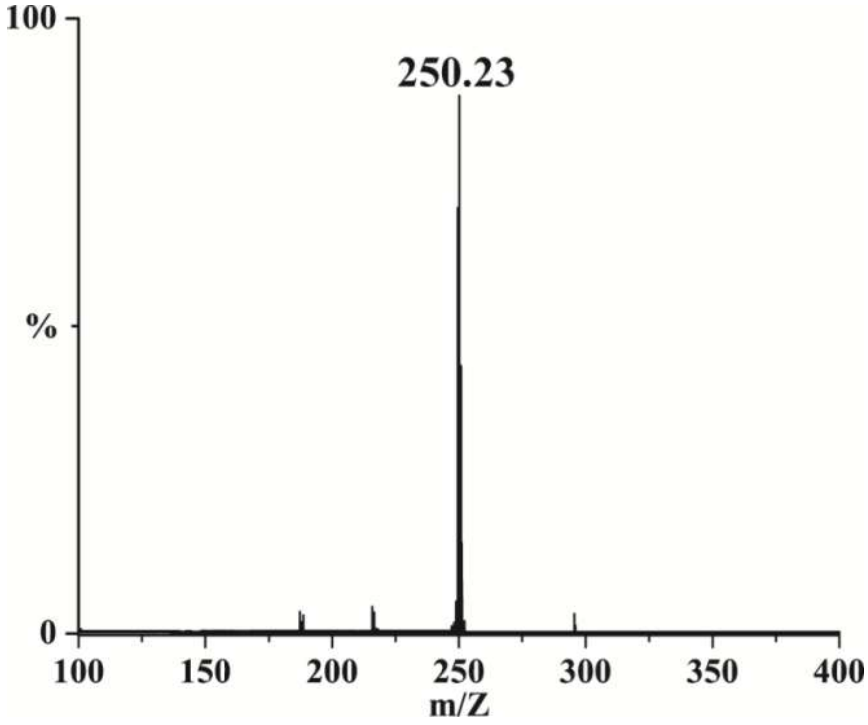

Figure S29: ESI-mass spectrum of 2, 4-di-*tert*-butyl-6-nitrophenol in methanol.

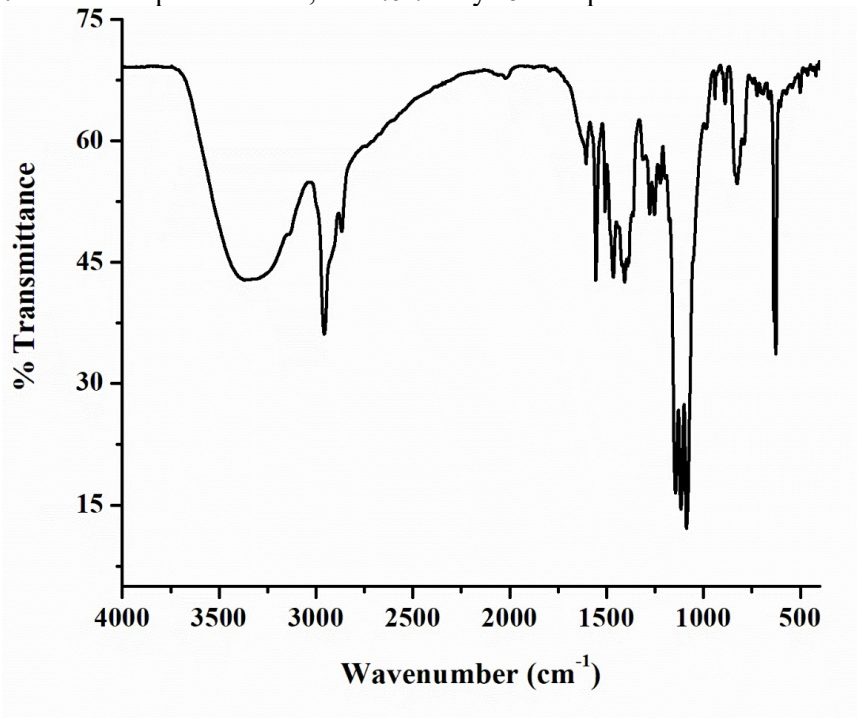

Figure S30: FT-IR spectrum of complex **5** in KBr.

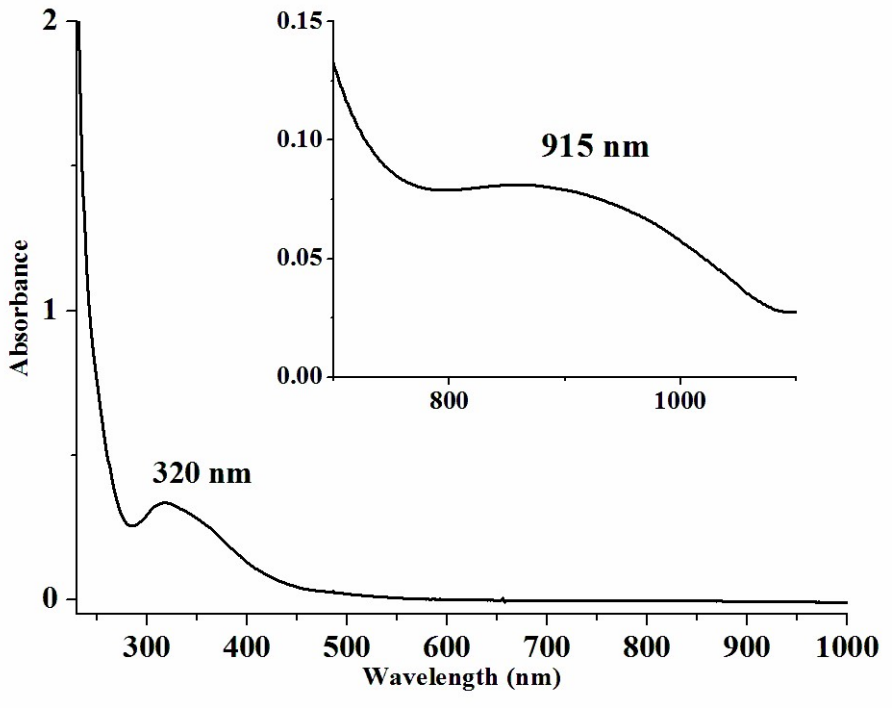

Figure S31: UV-visible spectrum of complex **5** in DMSO at RT.

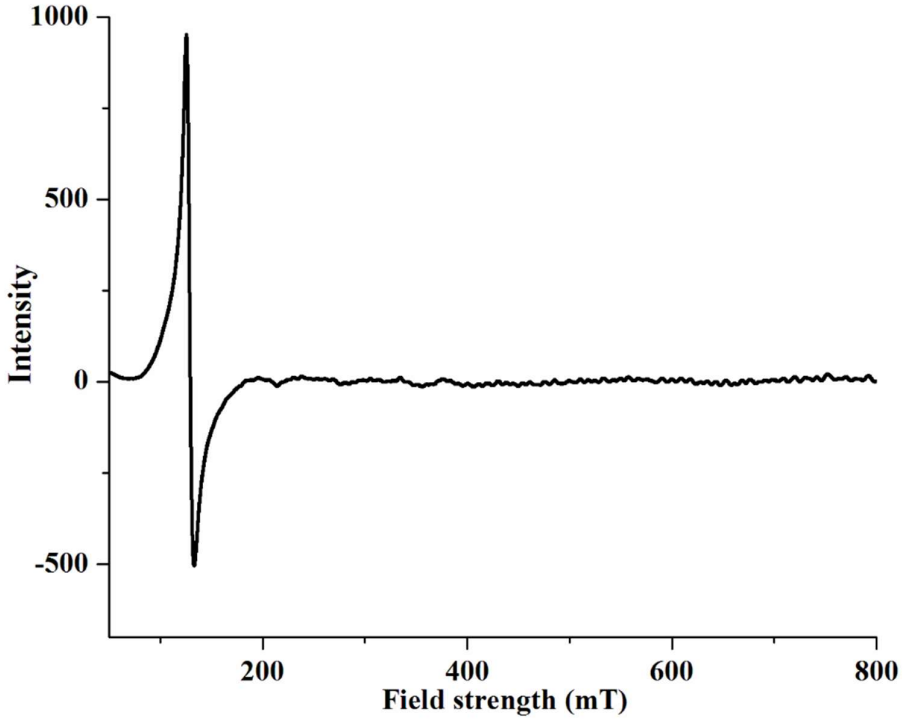

Figure S32: X-band EPR spectrum of complex **5** in DMSO at 77 K (g ~5.06).

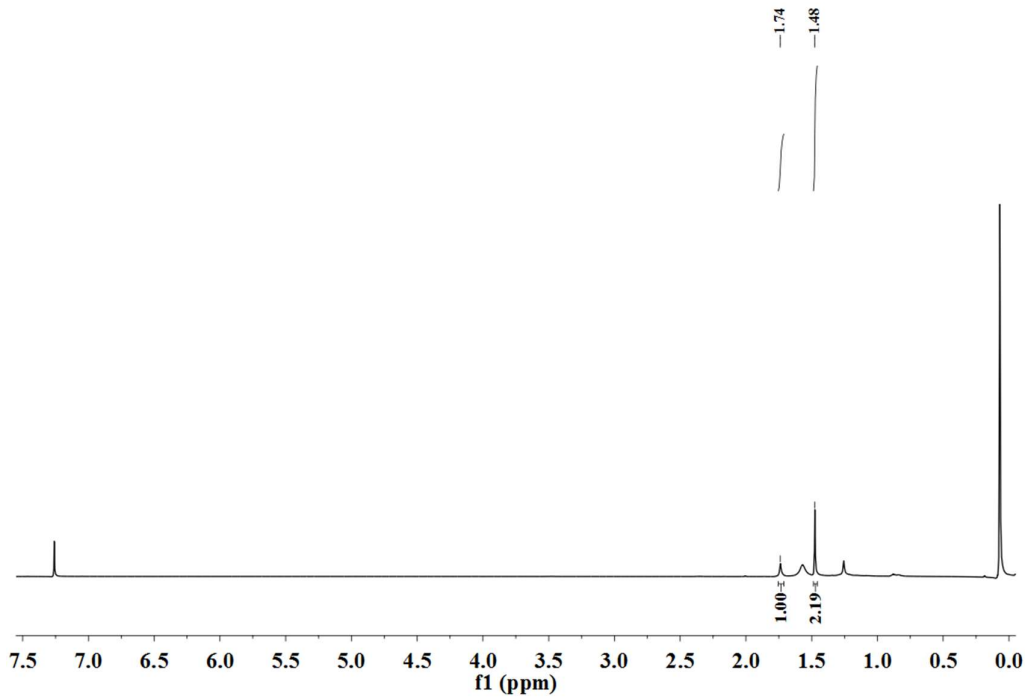

Figure S33: ^{1}H NMR spectrum of **($tmpH_2^+$)(NO_3^-)** in $CDCl_3$.

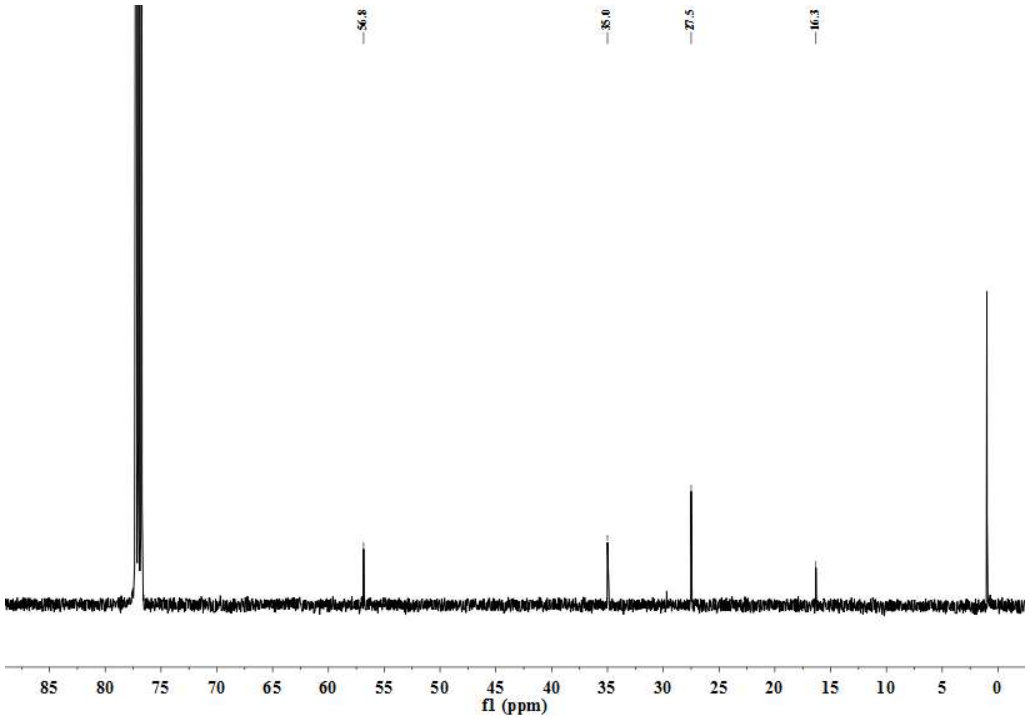

Figure S34: ^{13}C NMR spectrum of **($tmpH_2^+$)(NO_3^-)** in $CDCl_3$.

Table A1: Crystallographic data for complexes **1, 2, L′** and **($tmpH_2^+$)(NO_3^-)**

	1	**2**	**L′**	**($tmpH_2^+$)(NO_3^-)**
Formulae	$C_{20}H_{34}Cl_2N_8O_{10}Fe$	$C_{20}H_{30}Cl_2N_9O_9Fe$	$C_{15}H_{23}Cl_2N_7O_{10}$	$C_9H_{20}N_2O_3$
Mol. wt.	673.30	667.28	532.30	204.27
Crystal system	Triclinic	Monoclinic	Monoclinic	Orthorhombic
Space group	P -1	P 21/n	P 21	Pca21
Temperature /K	296(2)	101(2)	293(2)	293(2)
Wavelength /Å	0.71073	0.71073	0.71073	0.71073
a /Å	11.9018(6)	10.4501(6)	8.3825(5)	15.56(4)
b /Å	11.9774(6)	19.7521(12)	9.5056(5)	9.90(2)
c /Å	12.2326(6)	15.8247(9)	15.3798(8)	15.75(4)
α/°	84.555(3)	90	90	90
β/°	74.331(3)	91.422(4)	94.911(5)	90
γ/°	68.652(2)	90	90	90
V/ $Å^3$	1563.78(14)	3265.4(3)	1220.97(12)	2426(10)
Z	2	4	2	8
Density/Mgm^{-3}	1.430	1.357	1.448	1.118
Abs. Coeff. /mm^{-1}	0.714	0.682	0.328	0.083
Abs. correction	none	none	multi-scan	none
F(000)	700	1380	552	896
Total no. of reflections	5502	5764	3475	4258
Reflections, $I > 2\sigma(I)$	4355	3822	2853	2392
Max. 2θ/°	25.000	24.999	24.993	24.990
Ranges (h, k, l)	-14 ≤ h ≤ 14 -14 ≤ k ≤ 14 -14 ≤ l ≤ 14	-12 ≤ h ≤ 12 -23 ≤ k ≤ 23 -18 ≤ l ≤ 18	-9 ≤ h ≤ 7 -10 ≤ k ≤ 11 -17 ≤ l ≤ 18	-18≤ h ≤ 18 -11 ≤ k ≤ 11 -18 ≤ l ≤ 18
Complete to 2θ (%)	1.000	1.000	1.000	0.999
Refinement method	Full-matrix least-squares on F^2	Full-matrix least-squares on F^2	Full-matrix least-squares on F^2	Full-matrix least-squares on F^2
Goof (F^2)	1.012	1.024	1.026	1.023
R indices [$I > 2\sigma(I)$]	0.0564	0.0770	0.0641	0.0725
R indices (all data)	0.0723	0.1158	0.0780	0.1360

Table A2: Selected bond lengths (Å) of complexes **1, 2, L′** and **($tmpH_2^+$)(NO_3^-)**

Atoms	**1**	**2**	**L′**	**($tmpH_2^+$)(NO_3^-)**
Fe1-N1	2.161(4)	2.101(5)		
N1-N2	1.365(6)	1.354(6)	1.370(8)	
Fe1-N3	2.293(4)	2.330(4)		
Fe1-N8	2.118(5)	1.732(6)		
N8-O1		1.13(1)		

Fe1-N9		2.195(5)		
Fe1-O1	2.100(3)			
C1-C2	1.48(1)	1.476(9)	1.49(1)	1.549(1)
C2-C3	1.40(1)	1.395(9)	1.36(1)	
C3-C4	1.358(9)	1.379(9)	1.36(1)	
N1-C2	1.332(6)	1.343(8)		
N2-C2			1.357(9)	
Cl1-O3	1.417(7)	1.424(9)	1.36(1)	
Cl2-O7	1.412(5)	1.378(8)	1.372(7)	
N2-O1			1.50(1)	1.226(8)
N3-O1			1.442(9)	
N1-C1				1.552(1)
C1-C2				1.549(1)
C4-C5				1.563(13)
C5-C6				1.533(14)
C6-C7				1.511(11)
N2-O2				1.250(9)

Table A3: Selected bond angles (˚) of complexes **1, 2, L′** and **($tmpH_2^+$)(NO_3^-)**

Atoms	**1**	**2**	**L′**	**($tmpH_2^+$)(NO_3^-)**
N1-Fe1-N3	76.8(1)	76.0(2)		
N3-Fe1-N5	76.4(1)	75.3(2)		
N3-Fe1-N7	77.6(1)	77.1(2)		
N1-Fe1-N8	103.9(2)	104.3(2)		
Fe1-N8-O1		174.2(6)		
N1-Fe1-N9		86.2(2)		
N1-Fe1-O1	87.4(1)			
O3-Cl1-O4	106.6(4)	96.6(6)	109.2(7)	
O7-Cl2-O8	112.6(4)	116.5(7)	112.2(5)	
O1-N3-O2			117.9(6)	
N3-C7-N6			113.9(6)	
C6-N6-C8			118.3(6)	
N1-C1-C4				107.8(7)
C1-C4-C5				112.8(8)
C4-C5-C6				109.9(8)
O1-N2-O2				124.0(9)
O1-N2-O3				119.0(9)

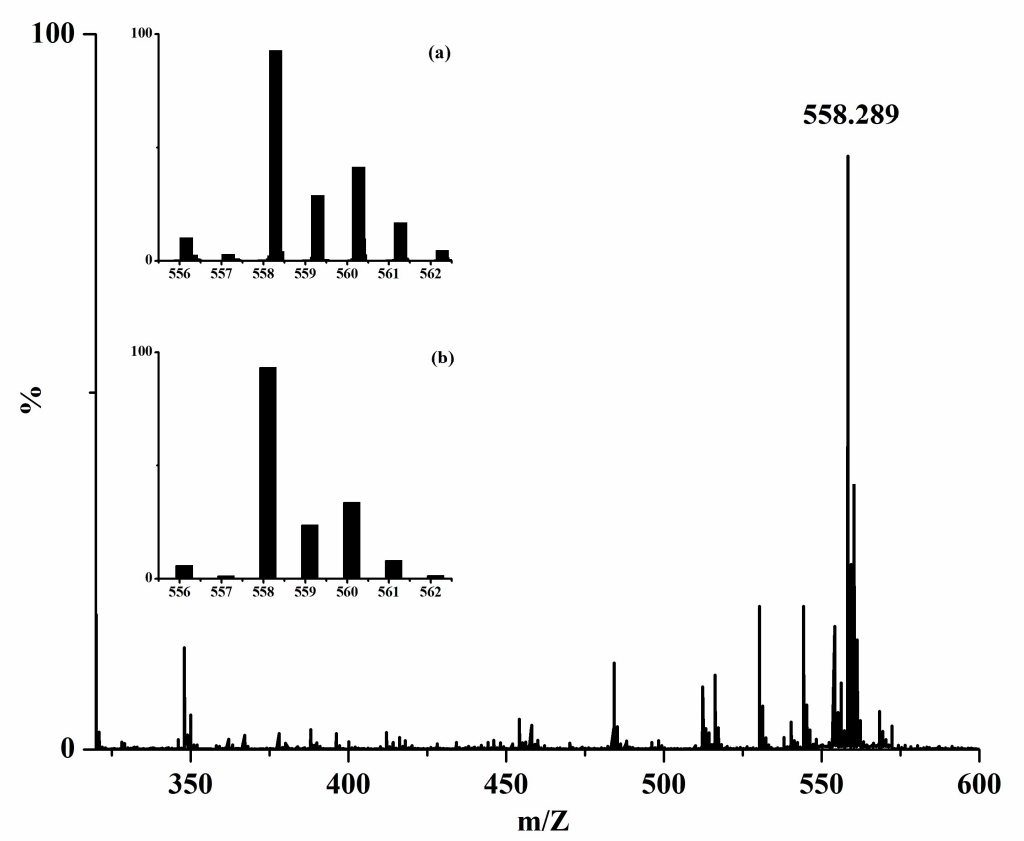

Figure S35. ESI-mass spectrum of complex **3** in acetonitrile. [Inset: (a) experimental and (b) simulated isotopic distribution pattern].

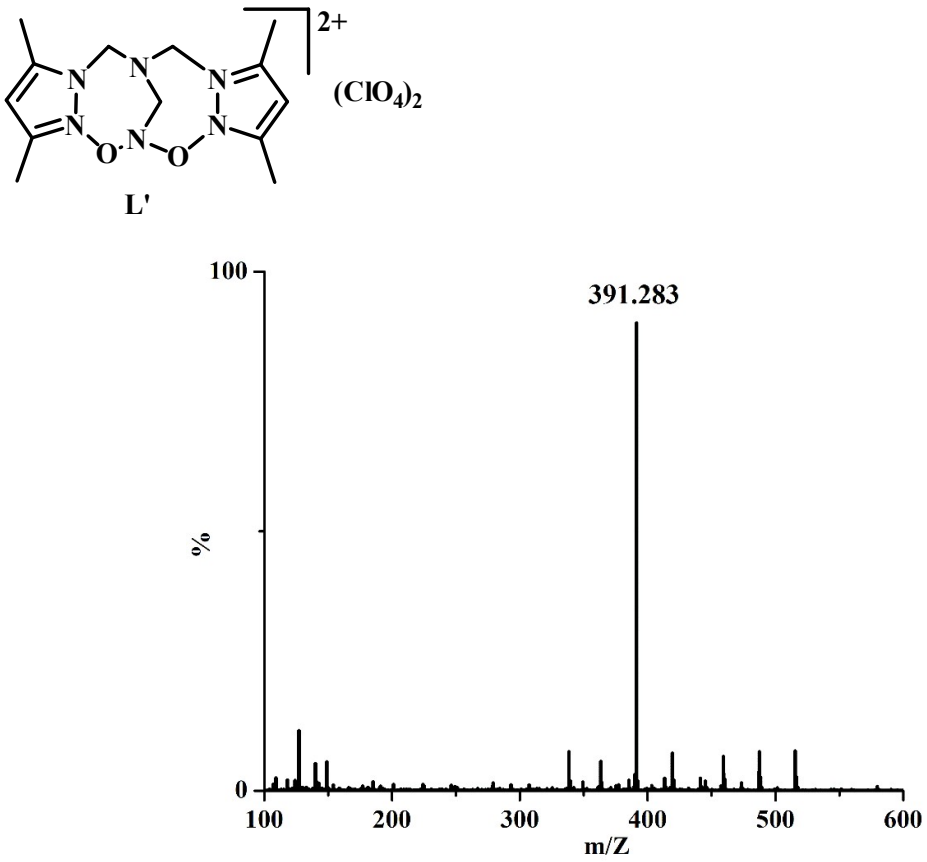

Figure S36: ESI-mass spectrum of modified ligand (L′) in acetonitrile.

ESI-mass of modified ligand: $[L'(ClO_4)]^+$ unit: calculated: 391.113; found: 391.283.

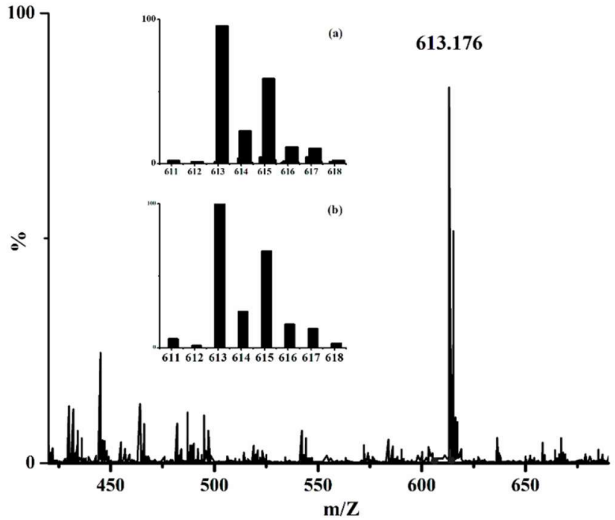

Figure S37. ESI-mass spectrum of complex **5** in acetonitrile. [Inset: (a) experimental and (b) simulated isotopic distribution pattern].

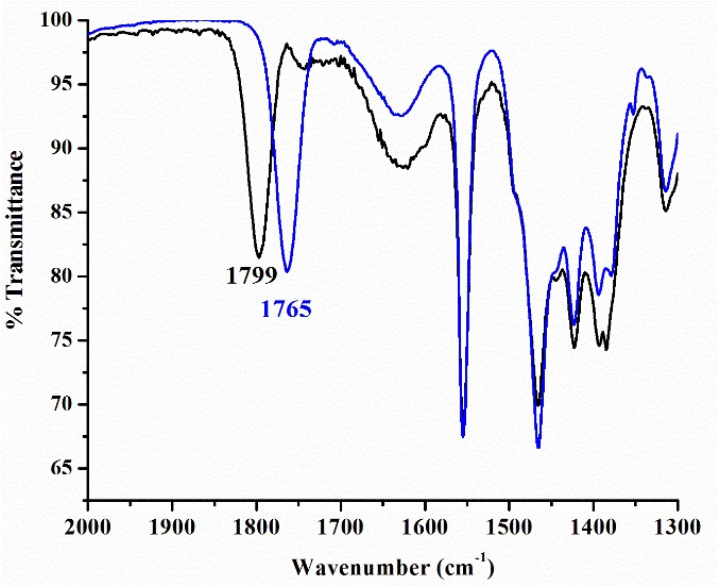

Figure S38: FT-IR spectra of reaction of complex **1** with NO gas (black line) and ^{15}NO gas (blue line) in acetonitrile medium at room temperature.

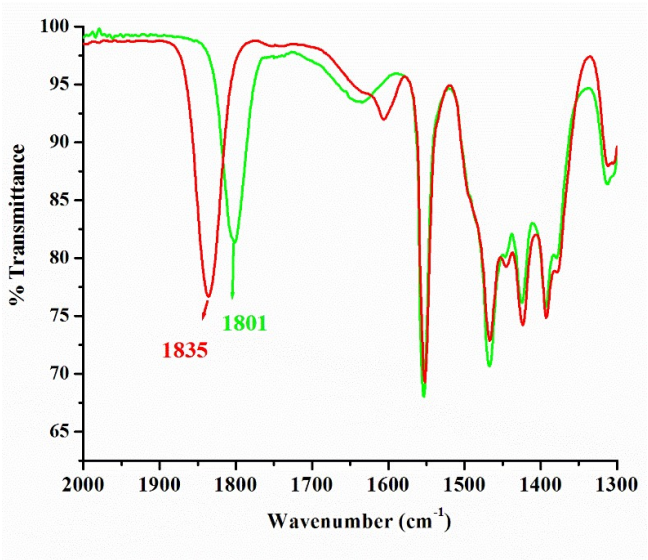

Figure S39: FT-IR spectra of $\{Fe(NO)\}^6$ formed in the reaction of complex **2** with O_2. Red trace represents with NO and green trace for it's ^{15}NO labelled analogue.

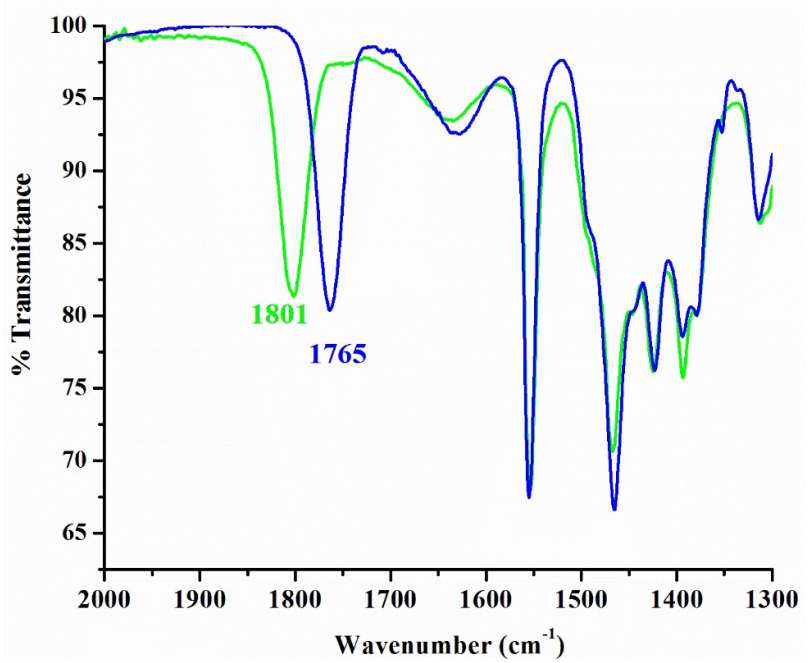

Figure S40: FT-IR spectral monitoring of the reaction of complex **2** (^{15}NO labeled) with O_2 in acetonitrile medium. [complex **2** (blue), after O_2 addition (green)].

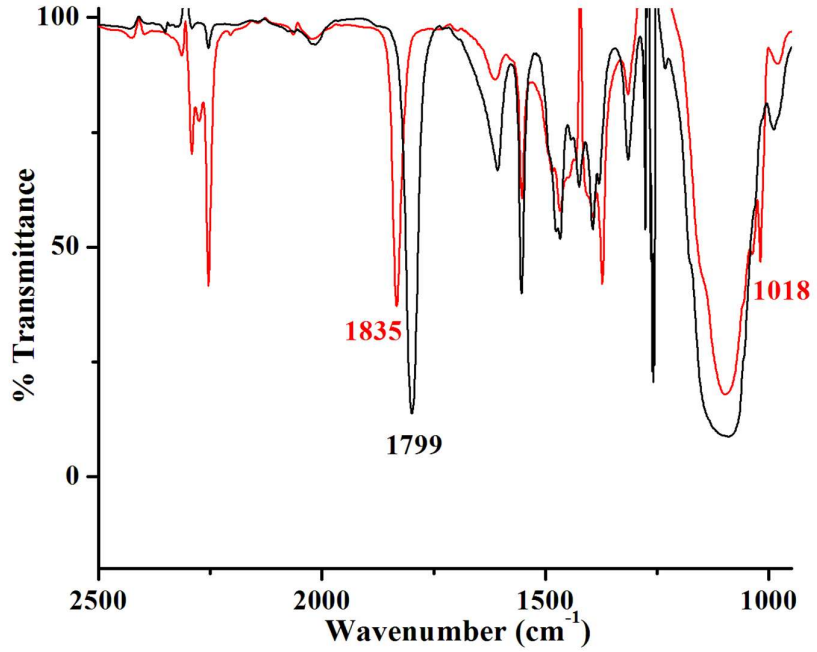

Figure S41: FT-IR spectral monitoring of the reaction complex **2** with $AgClO_4$ in acetonitrile medium.

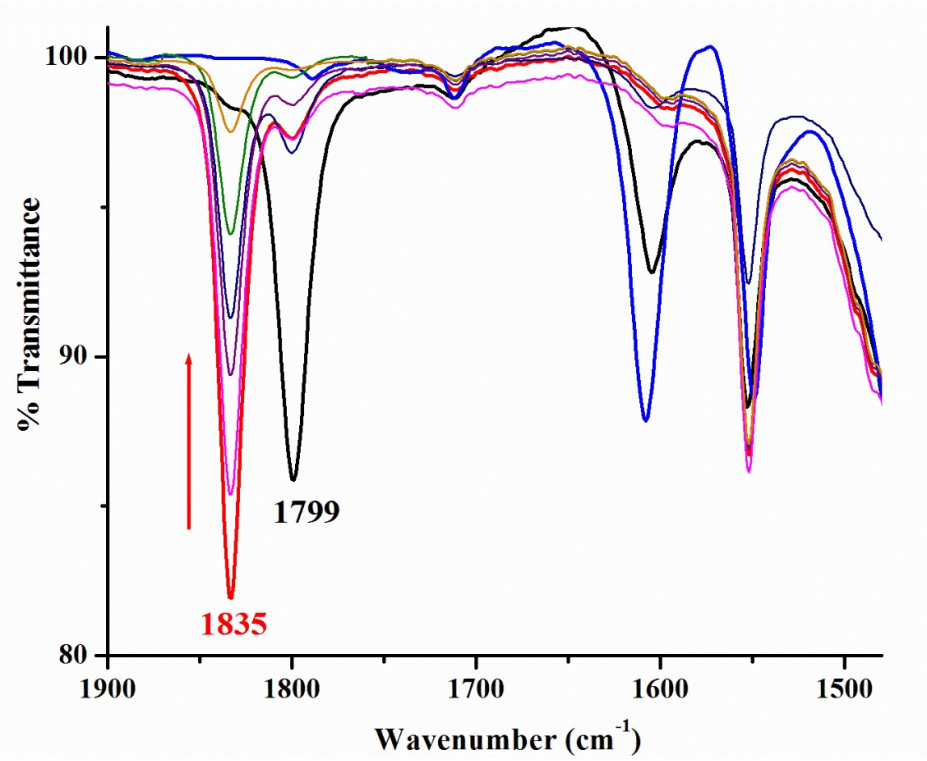

Figure S42: FT-IR spectral monitoring of the decomposition of $\{Fe(NO)\}^6$ intermediate in acetonitrile solution.